Acta Mechanica 177, 115–136 (2005)
DOI 10.1007/s00707-005-0229-z

Acta Mechanica
Printed in Austria

Direct numerical simulation of stably and unstably stratified turbulent open channel flows

Y.-H. Dong and **X.-Y. Lu,** Hefei, China

Received June 24, 2004; revised January 24, 2005
Published online: May 4, 2005

Summary. Direct numerical simulation of stably and unstably stratified turbulent open channel flow is performed. The three-dimensional Navier-Stokes and energy equations under the Boussinesq approximation are numerically solved using a fractional-step method based on high-order accurate spatial schemes. The objective of this study is to reveal the effects of thermally stable and unstable stratification on the characteristics of turbulent flow and heat transfer and on turbulence structures near the free surface of open channel flow. Here, fully developed weakly stratified turbulent open channel flows are calculated for the Richardson number ranging from 20 (stably stratified flow) to 0 (unstratified flow) and to -10 (unstably stratified flow), the Reynolds number 180 based on the wall friction velocity and the channel depth, and the Prandtl number 1. To elucidate the turbulent flow and heat transfer behaviors, typical quantities including the mean velocity, temperature and their fluctuations, turbulent heat fluxes, and the structures of velocity and temperature fluctuations are analyzed.

1 Introduction

Understanding and prediction of the interaction of turbulence with a free surface as well as heat or mass transfer near a free surface are of great importance in both applications and fundamentals. It is needed to explore more fundamental knowledge of the scalar transport processes near the interfacial surface and the interaction of turbulence with the surface. A natural and convenient way to investigate these flows is by use of a fully developed turbulent open channel flow, where the turbulence that arrives at the free surface is produced principally at the bottom solid wall. A variety of studies on open channel turbulence have been performed experimentally and computationally and will be briefly reviewed in the following.

Some typical experiments [1]–[7] have revealed that the most surface renewal events are due to bursting processes near the solid boundary, and verified that large-scale, energy-containing eddies are primarily responsible for surface renewal. A relatively simple scenario emerges from these experiments; low-speed fluid is ejected toward the surface from the bottom wall burst, the fluid rises to the surface to form a surface renewal patch, and a downdraft develops after the interaction.

Although those experiments have disclosed much about the processes involved in turbulent surface renewal, there exists a considerable difficulty in making accurate velocity and scalar measurements very near to the free surface. To some extent, an accurate numerical simulation can be employed to study this problem, allowing precise determination of the velocity field very close to the free surface. As is well known, a direct numerical simulation (DNS) approach can

be used to calculate and analyze the behaviors of turbulence structure and scalar transport near the free surface. Lam and Banerjee [8] conducted the first DNS of free surface flows with flat gas-liquid interface. Then, some DNS was performed to deal with turbulence structure in an open channel flow with a zero-shear gas-liquid interface [9]–[11]. Recently, DNS has also been carried out to investigate turbulence structure and scalar transport near the free surface in an open turbulent channel flow with a passive scalar. Nagaosa [12] studied the dynamics of well-organized tube-like coherent structures under a free surface and turbulent scalar transfer across the free surface in fully developed turbulent open channel flow at $\mathrm{Ri}_\tau = 150$ and $\mathrm{Pr} = 1$. Handler et al. [13] used the DNS to investigate fully developed turbulence in the open channel with passive heat transfer at $\mathrm{Ri}_\tau = 180$ and $\mathrm{Pr} = 2$, and found the importance of the interaction of turbulent structures in free surface with heat transport. Handler et al. [14] further performed the DNS to deal with the effects of surfactants on heat transfer and the underlying turbulent structures. They found that, as surface elasticity is increased, turbulent fluctuations are damped and the mean surface temperature is decreased. Shen et al. [15], [16] investigated numerically and analytically the mixing of a passive scalar in turbulent shear flow with a free surface.

The turbulence structure near the free surface is considerably affected when an active scalar (e.g., thermal energy) is transferred across the free surface. Based on previous works [17]–[19], it is found that turbulence statistics in stably stratified flows depends on the local Richardson number, defined by the local velocity and temperature gradients, and the effect of thermal stratification is significant in the scalar transfer into turbulent flows. As remarked by Nagaosa and Saito [20], the turbulence structure and scalar transfer near the free surface in stratified flows are complicated since the stratification influences the turbulence structure, in particular in the turbulent boundary layer near the wall. To the best of our knowledge, however, little work for thermally stratified open turbulent channel flows has been performed to deal with the turbulence structure near the free surface. Only Nagaosa and Saito [20] have investigated stably stratified open turbulent channel flow based on DNS approach. Therefore, the influence of the thermal stratification on the scalar transfer across the free surface is still not well known. Investigations of the details of the turbulence structures and scalar transfer mechanisms in stably and unstably stratified flows are necessary. Thus, in this study, stably and unstably stratified turbulent open channel flows are investigated by solving the three-dimensional Navier-Stokes and energy equations under the Boussinesq approximation by use of a fractional-step method coupled with the high-order accurate spatial schemes.

This paper is organized as follows. The mathematical formulation is described in Sect. 2. The numerical method and its validation are given in Sect. 3. In Sect. 4, some typical statistical quantities including the mean velocity, temperature and their fluctuations, turbulent heat fluxes, and the structures of the instantaneous velocity and temperature fluctuations are discussed. Finally, concluding remarks are summarized in Sect. 5.

2 Mathematical formulations

To investigate a fully developed turbulent open channel flow with heat transfer near a free surface in the absence of significant surface deformation effect, the governing equations are the three-dimensional filtered incompressible Navier-Stokes and energy equations under the Boussinesq approximation. To make the equations dimensionless the channel depth δ is used as the length scale, the wall friction velocity u_τ as the velocity scale, and the temperature difference ΔT as the temperature scale, where ΔT is defined as $\Delta T = T_F - T_B$ for stable stratification and

$\Delta T = T_B - T_F$ for unstable stratification, with T_F and T_B being the temperature at the free surface and at the bottom wall, respectively. The nondimensional governing equations are given as

$$\frac{\partial u_i}{\partial x_i} = 0, \tag{1}$$

$$\frac{\partial u_i}{\partial t} + \frac{\partial}{\partial x_j}(u_i u_j) = -\frac{\partial p}{\partial x_i} + \frac{1}{\mathrm{Re}_\tau}\frac{\partial^2 u_i}{\partial x_j \partial x_j} + \delta_{i1} + Ri_\tau \tilde{T}\delta_{i2}, \tag{2}$$

$$\frac{\partial T}{\partial t} + \frac{\partial (T u_j)}{\partial x_j} = \frac{1}{\mathrm{Re}_\tau \mathrm{Pr}}\frac{\partial^2 T}{\partial x_j \partial x_j}, \tag{3}$$

where u_i $(i = 1,\ 2,\ 3)$ is the velocity, and is for writing convenience represented as u, v and w in the streamwise (x), vertical (y) and spanwise (z) direction, respectively. p and T are the pressure and temperature. The Reynolds number Re_τ is defined as $\mathrm{Re}_\tau = u_\tau \delta / v$, the Richardson number Ri_τ is defined as $\alpha g \Delta T \delta / u_\tau^2$, and the Prandtl number Pr as $\mathrm{Pr} = v/\kappa$ with v being the kinematic viscosity, κ the thermal diffusivity of the fluid, α the thermal expansion coefficient, and g the gravitational acceleration. $\tilde{T} = T - < T >_S$, and $<>_S$ stands for an average over a plane parallel to the horizontal wall.

In this study, the no-slip velocity condition is imposed at the bottom wall $y = 0$. The boundary conditions applied at $y = 1.$ are those for a shear-free interface without deformation, i.e.,

$$v = 0, \quad \frac{\partial u}{\partial y} = \frac{\partial w}{\partial y} = 0. \tag{4}$$

The flow and temperature fields are assumed to be statistically homogeneous in the streamwise and spanwise directions. Thus, periodic boundary conditions are employed in both the directions. For stably stratified channel flow, two different constant temperatures with the top temperature being greater than the bottom are imposed,

$$T = T_F = 0.5 \ \text{ at } y = 1, \quad T = T_B = -0.5 \ \text{ at } \ y = 0. \tag{5.1}$$

For unstable stratification, the constant temperatures with the bottom temperature being greater than the free surface are set,

$$T = T_F = -0.5 \ \text{ at } y = 1, \quad T = T_B = 0.5 \ \text{ at } \ y = 0. \tag{5.2}$$

Thermally stratified turbulent computation is started after the flow field has statistically reached a fully developed turbulent state. The initial temperature field is set to be a linear distribution along the vertical direction and homogeneous in the horizontal planes.

Usually, the Richardson number Ri_τ is used to characterize the buoyancy effect in stably and unstably stratified flows. Based on the nondimensional temperature scale described in the above and the boundary conditions (5.1) and (5.2), Ri_τ for stable and unstable stratification is positive. It is needed to notice that, for the writing and discussing convenience, we represent Ri_τ for unstable stratification as the corresponding negative value here.

3 Numerical methods

To perform DNS for stably and unstably stratified turbulent open channel flows, a fractional-step method [21], coupled with the high-order finite-difference schemes developed by Rai and Moin [22], is employed to solve Eqs. (1)–(3). As indicated by Rai and Moin [22], the approach based on the high-order accurate schemes is a good candidate for direct simulations of

turbulent flows, because results calculated appear far superior to those obtained with conventional second-order schemes and are found to compare very well with spectral simulations. Time advancement is carried out by the semi-implicit scheme mixing the second-order Crank-Nicholson scheme for the viscous terms and the third-order Runge–Kutta scheme for the convective terms. So, the algorithm is overall second-order accurate in time but the low-storage Runge–Kutta methods have the additional advantage that the minimum amount of computer run-time memory is realized. The discretized formulation was described in detail in [21] and [22].

In this study, the size of the computational domain is $2\pi\delta \times \delta \times 3\pi\delta/2$ with the corresponding grid size $128\times129\times128$ in three directions. The domain size is chosen such that two-point correlations in both the streamwise and spanwise directions are negligibly small. The grid independence of the present calculation has been ensured for every simulation. The grid is uniform along both the streamwise and spanwise directions. In the vertical direction, the mesh is stretched to increase the grid resolution near the free surface and bottom wall, so that the grid distribution is sufficient to resolve the viscous sublayer and diffusive sublayer near the boundaries.

To validate the present calculation quantitatively, stably stratified turbulent open channel flows are calculated and compared to some typical DNS results [20]. Here, two cases with $\mathrm{Ri}_\tau = 10$ and 20, $\mathrm{Re}_\tau = 150$ and $\mathrm{Pr} = 1$, which were investigated by Nagaosa and Saito using DNS, are calculated. The distributions of the mean velocity normalized by the friction velocity and the streamwise, vertical and spanwise velocity fluctuations relative to the bulk-mean velocity u_b are shown in Fig. 1. It is seen that our calculated results agree with the DNS data [20]. Although the peak values of the vertical and spanwise velocity fluctuations are somewhat higher than the results in [20], it can be explained as that the present code with the higher-order schemes can more reasonably predict the turbulent flow behaviors. Moreover, we have compared other turbulent quantities with some previous DNS results (not shown here) and can confirm that our calculation code enables the DNS results to be satisfactory. To demonstrate that the computed results are independent of the time steps and the grid sizes, the results calculated by different grid sizes and time steps are also shown in Fig. 1.

Further, to verify the performance of the present DNS calculation, a fully developed turbulent open channel flow at $\mathrm{Re}_\tau = 180$ is investigated and compared to DNS results [13] and experimental data [9], as shown in Fig. 2a and b for the mean velocity and the streamwise, vertical and spanwise velocity fluctuations. It is seen that our calculated result is in good agreement with those results [9], [13]. To ensure the present DNS calculation for high-order correlation terms, as shown in Fig. 2c and d, it is evident that the skewness and flatness profiles for all velocity components are in good agreement with previous results [13]. The present computational method and the relevant code have also been validated and verified in our previous work [23]–[26]. Thus, it can be confirmed that our calculation is reliable for the prediction of statistical quantities of the turbulent flow and heat transfer for stably and unstably stratified turbulent open channel flows.

4 Results and discussion

4.1 Velocity statistics and turbulence intensities

For thermally stratified turbulent open channel flow, the buoyancy force has a significant influence on the vertical turbulent transport and internal energy conversion between turbulent

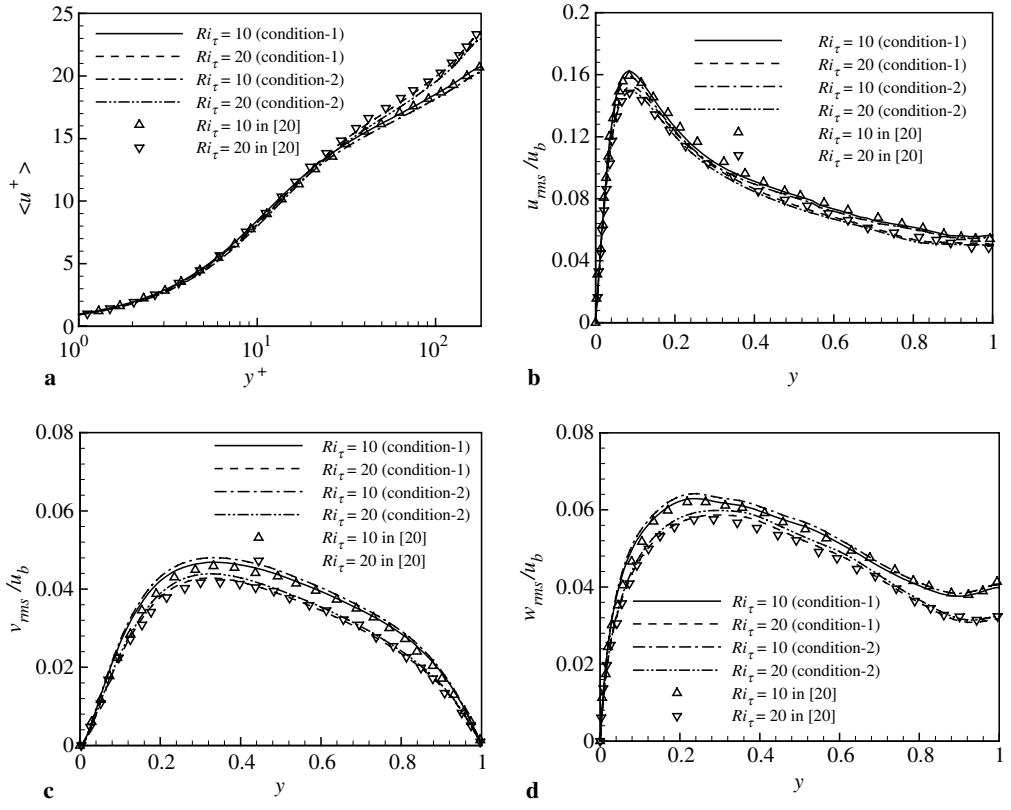

Fig. 1. Distributions of the mean velocity **a** and its fluctuations in the streamwise **b**, vertical **c**, and spanwise **d** direction and their comparison with previous DNS results [20]. Condition-1: grid size 128 × 129 × 128 and time step 0.001; Condition-2: grid size 256 × 257 × 256 and time step 0.0005

kinetic energy and turbulent potential energy. The velocity and temperature fields are coupled and affect each other. Figure 3 shows the mean streamwise velocity for the turbulent open channel flow versus y^+, where y^+ is the vertical distance from the bottom wall normalized by the friction velocity and is defined as $y^+ = yu_\tau/v$. Based on previous studies [10]–[13], the velocity statistics near the no-slip boundary are nearly not affected by the existence of a free surface. In the sublayer, $y^+ < 10$, the results follow the linear law of the wall quite well. In the region of $y^+ > 20$, as Ri_τ increases from 0 to 20 for the cases of stably stratified turbulent flow, the flow speeds up and the centerline velocity increases. Clearly, the bulk mean velocity u_b increases with increasing Ri_τ although the friction velocity on the bottom wall is not changed. This is evidence that the turbulent boundary layer shows the tendency of re-laminarization in stably stratified flows. Such characteristics are consistent with the results predicted for stably stratified turbulent channel flows [20], [27], [28]. Meanwhile, as Ri_τ decreases from 0 to -10 for the cases of unstably stratified turbulent flow, the velocity profile develops gradually to a blunt distribution due to the unstable stratification effect, and as expected, the bulk mean velocity decreases with decreasing Ri_τ.

A logarithmic region in the stratified boundary layer appears based on the work performed by Garg et al. [27] and Arya [29]. Then, by examining the profiles in Fig. 3, the velocity distributions have a logarithmic form,

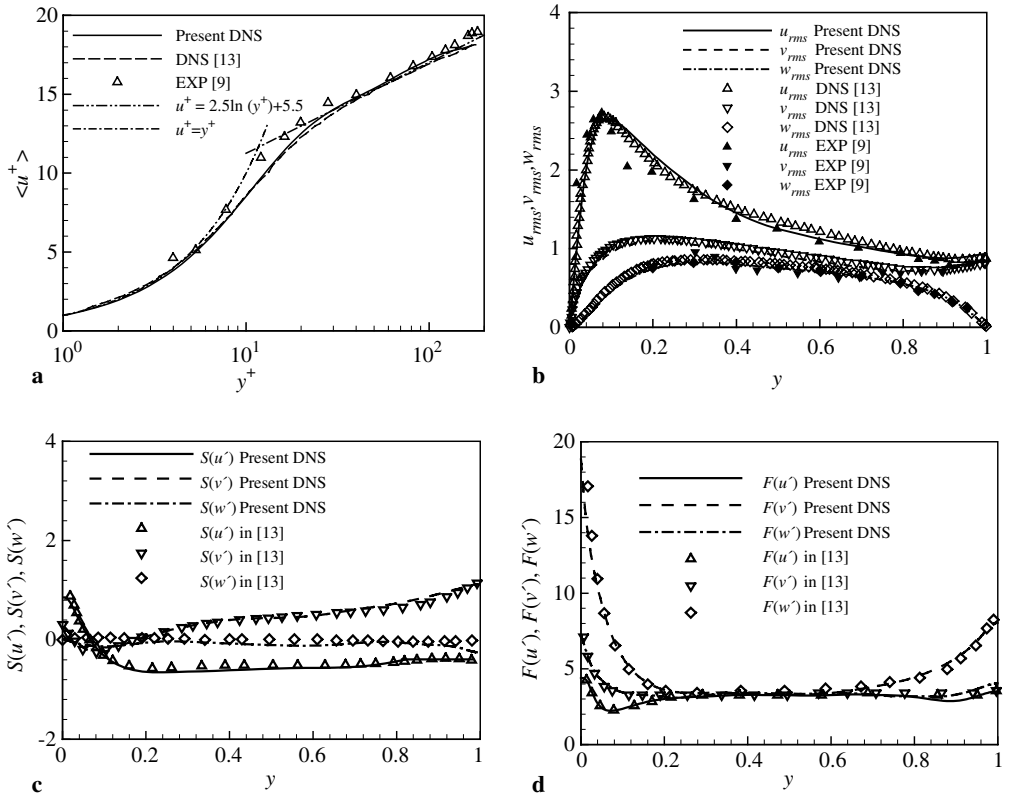

Fig. 2. Distributions of the mean velocity **a**, velocity fluctuations **b**, the skewness **c**, and flatness **d** profiles of velocity and their comparison with previous DNS results [13] and experimental data [9]

$$\langle u^+ \rangle = (1/K) \ln y^+ + B, \tag{6}$$

where K and B represent the von Kárman constant and the additive constant in the log law of the velocity profile, respectively, and $< >$ denotes an averaging in time and in the plane parallel to the wall plate. It is found that K and B depend on the Richardson number Ri_τ, which is closely related to the turbulent flow influenced by stable and unstable stratification. Based on logarithmic fits to the velocity profiles shown in Fig. 3, the parameters obtained are shown in

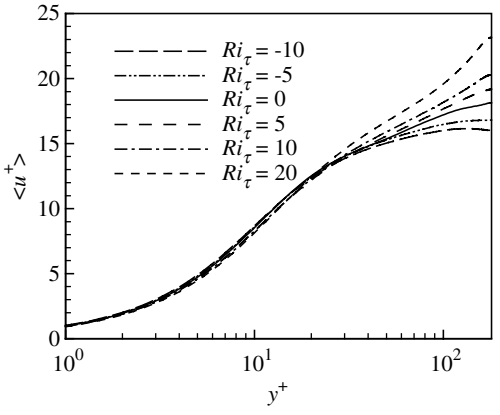

Fig. 3. Profiles of the mean streamwise velocity for different Richardson numbers

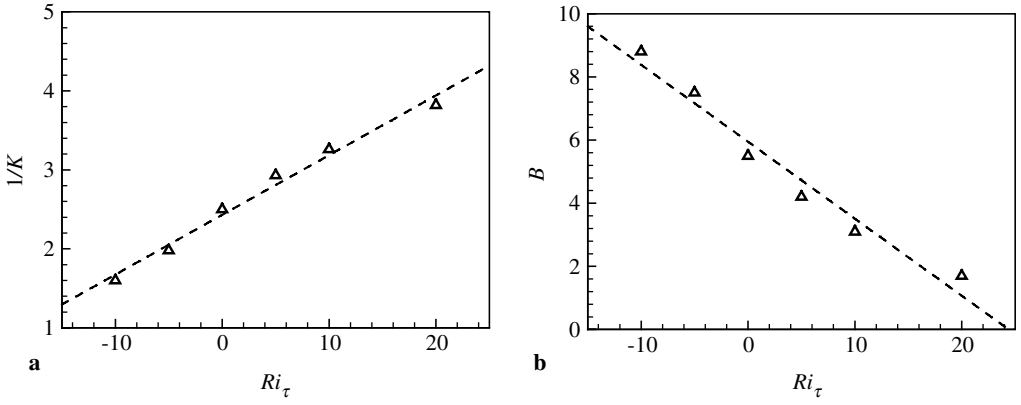

Fig. 4a. The von Kárman constant K, and **b** the additive constant B versus the Richardson number

Fig. 4 as functions of Ri_τ along with curve fits. When Ri_τ increases from -10 (i.e., unstable stratification) to 20 (i.e., stable stratification), both K and B decrease. Meanwhile, fitted linear relationships of K and B with Ri_τ are also plotted in Fig. 4. According to Prandtl's mixing length model [30], the turbulent eddy viscosity in the logarithmic layer is $\nu_T \sim l_m |d < \bar{u} > /dy|^2$, where $l_m \approx Ky$ is the mixing length. Under stable stratification, turbulence intensities are suppressed and the vertical length scale decreases, which is accounted for by decreasing K. In contrast, however, under unstable stratification, turbulence intensities are enhanced and the vertical length scale increases with the increase of K. This behavior is qualitatively consistent with results for stably stratified turbulent channel flows [27].

The turbulence intensity profiles, i.e., the root-mean-square values of the velocity fluctuations, relative to the bulk-mean velocities are shown in Fig. 5. The turbulence intensities show a strong anisotropy near the shear free boundary. The mechanism of the anisotropic behavior is analyzed based on the turbulence kinetic energy and dissipation budgets in the following. Here, the characteristics of the turbulence intensities versus Ri_τ are mainly discussed. For $\mathrm{Ri}_\tau = 5,\ 10$ and 20, in the turbulent boundary layer near the bottom wall the turbulence intensities in each direction decrease considerably due to stable stratification. The tendency of re-laminarization of the turbulent boundary layer is characterized by the decrease of the turbulence intensities. Meanwhile, for $\mathrm{Ri}_\tau = -5$ and -10, the turbulence intensities are increased due to unstable stratification. From the profiles of the turbulence intensities, the structure of the turbulent boundary layer near the wall is considerably affected by the stratification. Thus, the interaction between the organized structure in the turbulent boundary layer and the surface-renewal motions near the free surface, in particular for unstable stratification, is obviously observed in the stratified turbulent flows and will be discussed in the following.

To demonstrate the behavior of high-order correlation terms of the velocity fluctuation, a typical case is shown in Fig. 2c and d for $\mathrm{Ri}_\tau = 0$. The skewness $S(w')$ is near zero over the channel, indicating that the sample size is adequate for the computation of higher-order statistics. From Fig. 2c, it is clear that for $y > 0.15$ the skewness $S(v')$ is always positive and $S(u')$ is always negative. In fact, in the vicinity of the free surface for $y > 0.8$, the skewness $S(v')$ shows an increase. Thus, the largest number of intense motions near the interface are those for which the vertical velocity is positive, i.e., fluid motion toward the surface, and the streamwise fluctuations are negative. This is certainly consistent with the experimental observations of ejections of low-speed fluid originating from the solid

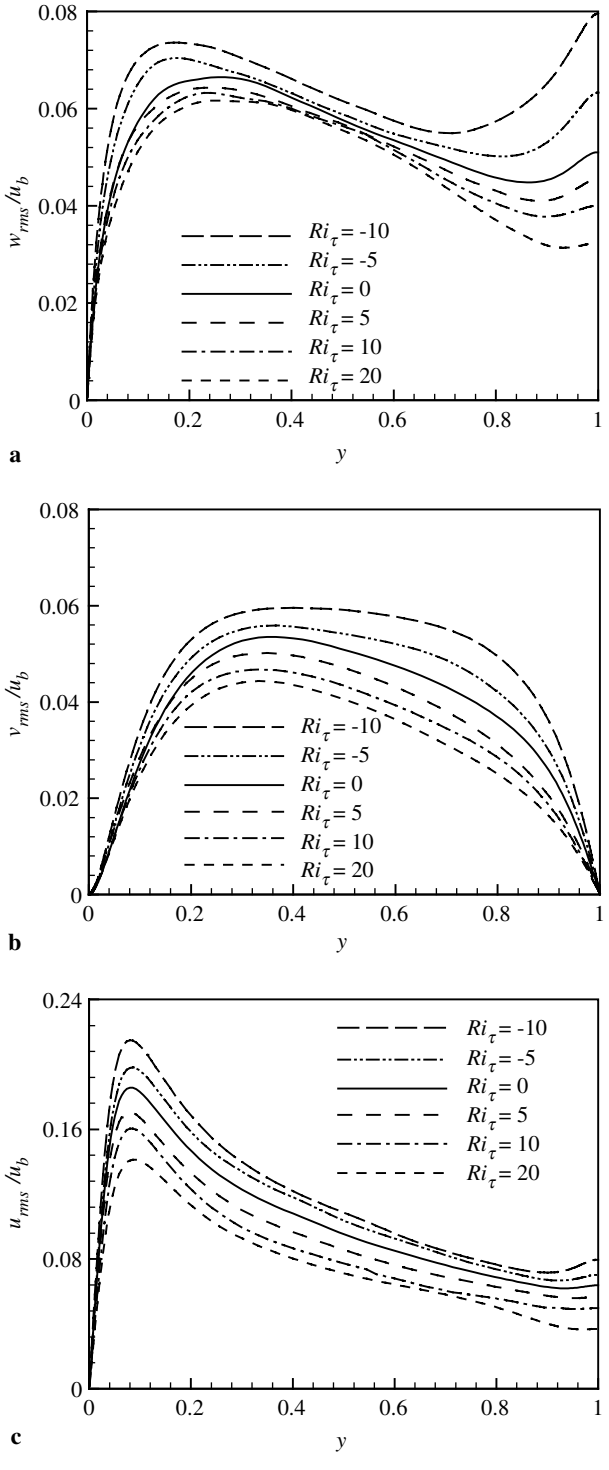

Fig. 5. Profiles of the streamwise, vertical and spanwise velocity fluctuations relative to the bulk-mean velocities for different Richardson numbers

boundary impinging on the surface. From Fig. 2d, it is evident that near the shear-free boundary the flatness $F(v')$, which attains a high level, deviates significantly from Gaussian

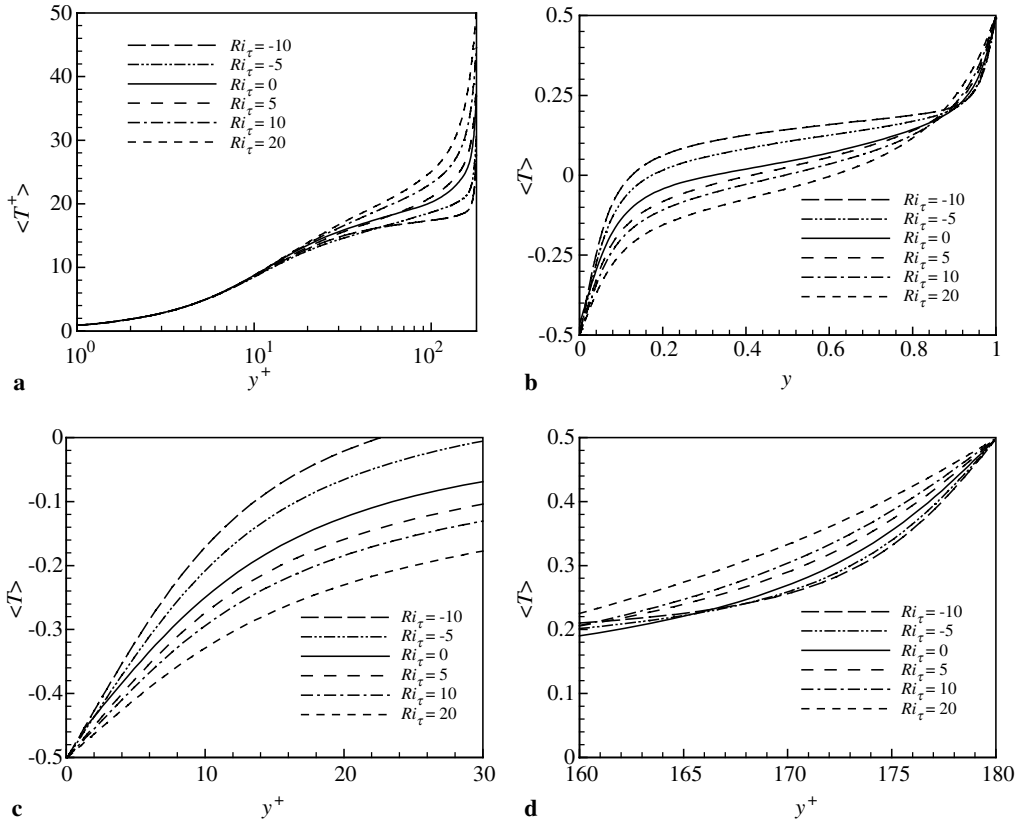

Fig. 6. Profiles of the mean temperature: **a** temperature normalized by friction temperature at the bottom wall, **b** over the channel, **c** near the bottom wall, **d** near the free surface

behavior. On the other hand, the flatness for the other velocity components deviates only slightly from Gaussian statistics.

Further, the skewness and flatness profiles of three velocity components for $\mathrm{Ri}_\tau = 10$ and -10 (not shown here) are also examined. Based on the calculated results, the skewness $S(v')$ exhibits an increase in the vicinity of the free surface for both $\mathrm{Ri}_\tau = 10$ and -10, and the value of $S(v')$ at the free surface for $\mathrm{Ri}_\tau = -10$ is higher than that for $\mathrm{Ri}_\tau = 10$. Thus, the fluid motion toward the surface is stronger for $\mathrm{Ri}_\tau = -10$, which is closely related to the ejections of the fluid originating from the solid boundary impinging on the surface. Meanwhile, the flatness $F(v')$ attains a high level and deviates from Gaussian behavior for $\mathrm{Ri}_\tau = 10$ and -10.

4.2 Temperature statistics and heat fluxes

Figure 6 shows the mean temperature profiles for different Ri_τ numbers. To clearly depict the mean temperature profiles for stable and unstable stratification, the mean temperature profiles are described as

$$\begin{aligned} &< T^+ >= [<T(y) > -T_B]/T_\tau \ , \ < T >=< T(y) > -T_B, \quad \text{for stable stratification,} \\ &< T^+ >= [T_B - < T(y) >]/T_\tau, < T >= T_B - < T(y) >, \quad \text{for unstable stratification,} \end{aligned} \tag{7}$$

where T_τ is the friction temperature and is defined as

$$T_\tau = \frac{\kappa}{u_\tau}\left|\frac{\partial < T >}{\partial y}\right|_{y=0}. \tag{8}$$

As shown in Fig. 6a, similar to the mean velocity distribution in Fig. 3, there exists a buffer layer followed by a logarithmic region in the mean temperature profile, where $< T^+ >$ behaves as

$$< T^+ >= (1/K_T)\ln y^+ + B_T, \tag{9}$$

where K_T and B_T represent the von Kárman constant and the additive constant in the log law of the mean temperature profile. It is found that K_T and B_T also depend on Ri_τ. For unstratified turbulent flow, i.e., $\mathrm{Ri}_\tau = 0$, Kader and Yaglom [31] found that $1/K_T = 2.12$ approximately, while Kader [32] gave an empirical expression for the function B_T that describes the experimental results in the logarithmic region of the fully turbulent boundary layer. Based on our careful checking the logarithmic fits to the temperature profiles in Fig. 6a, as Ri_τ increases from -10 (i.e., unstable stratification) to 20 (i.e., stable stratification), similar to the mean velocity behavior in Fig. 4, both K_T and B_T decrease. To exhibit the global behavior of the mean resolved temperature, Figs. 6b–d show the mean temperature profiles over the channel, near the wall and near the free surface, respectively.

The Nusselt number is an important parameter relevant to the heat transfer coefficient and is defined at the free surface as

$$\mathrm{Nu} = \frac{q_F \delta}{k\Delta T}, \tag{10}$$

where q_F represents the averaged heat flux through the free surface, and k is the thermal conductivity. As is well known, in the case of purely diffusive heat transport through a stationary fluid, $\mathrm{Nu} = 1$; thus the value of Nu quantifies the increase of heat transport at a wall or across a free surface due to turbulence with respect to its laminar value. Then, based on the mean temperature profiles in Fig. 6d, the Nusselt number is obtained and shown in Fig. 7 for Nu versus Ri_τ. It is found that a linear relationship between Nu and Ri_τ appears approximately for the range of Ri_τ considered in this study, which corresponds to the regime of the weakly stratified turbulent flows. Nu decreases with the increase of Ri_τ from -10 to 20. This behavior is quite rational because stable stratification dissociates the surface-renewal motions and restrains the heat transfer at the free surface, and, in contrast, unstable stratification enhances the heat transfer. Based on the DNS of stably stratified free surface turbulent flow [20], it is evident that the Richardson number rather than the Reynolds number has a significant influence on the heat transfer across the free surface. Komori et al. [2] and Rashidi et al. [6]

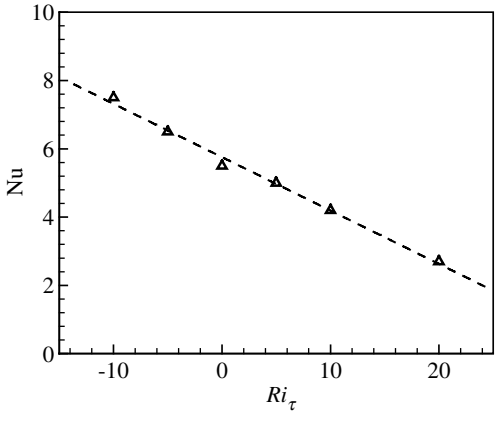

Fig. 7. Nusselt number at the free surface versus the Richardson number

investigated the passive heat transfer at the free surface and obtained a general relationship between the Reynolds number and the Nusselt number. At $\mathrm{Ri}_\tau = 0$, our calculated data $\mathrm{Nu} = 5.7$ approximately agrees well with $\mathrm{Nu} = 5.6$ [20] and 6.0 [6].

Figure 8 shows the profiles of the mean temperature fluctuation near the free surface and the bottom wall, where $y_F^+ = (1-y)u_\tau/\nu$, representing the vertical distance from the free surface normalized by the friction velocity. It is seen that the temperature fluctuation local maximum near the free surface is higher than that near the bottom wall; this phenomenon is consistent with previous work [13], [16]. When Ri_τ increases from -10 to 20, the amplitudes of the local maximum near both the free surface and the wall decrease. In the vicinity of the bottom wall, the results appear to be in agreement with those for stably stratified turbulent channel flows [27], [28]. As the distance from the wall goes to zero, the fluctuations of temperature approach zero linearly with a slope varying with Ri_τ in Fig. 8a.

To reveal the character of the mean turbulent heat transfer, Fig. 9 shows the profiles of the mean vertical turbulent heat flux ($< T'v' >$) near the free surface and the wall. Note that to exhibit clearly the mean turbulent heat transfer profiles for stable and unstable stratification, the absolute value of $< T'v' >$ for $\mathrm{Ri}_\tau \geq 0$ is plotted in Fig. 9. As Ri_τ increases from -10 to 20, the absolute value of the heat flux $< T'v' >$ decreases, in particular near the free surface. The

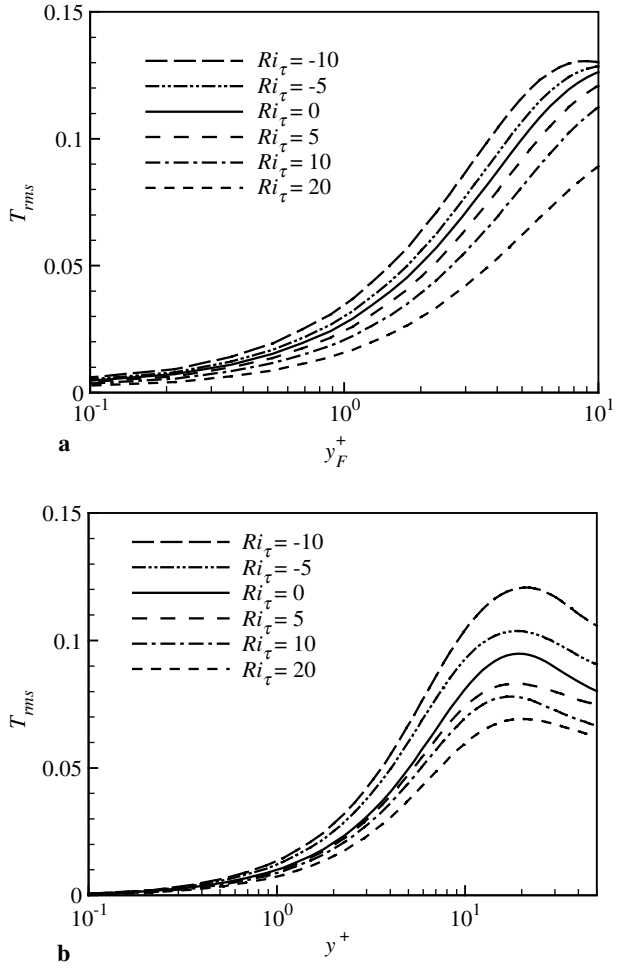

Fig. 8. Profiles of the mean temperature fluctuation **a** near the free surface, and **b** near the bottom wall

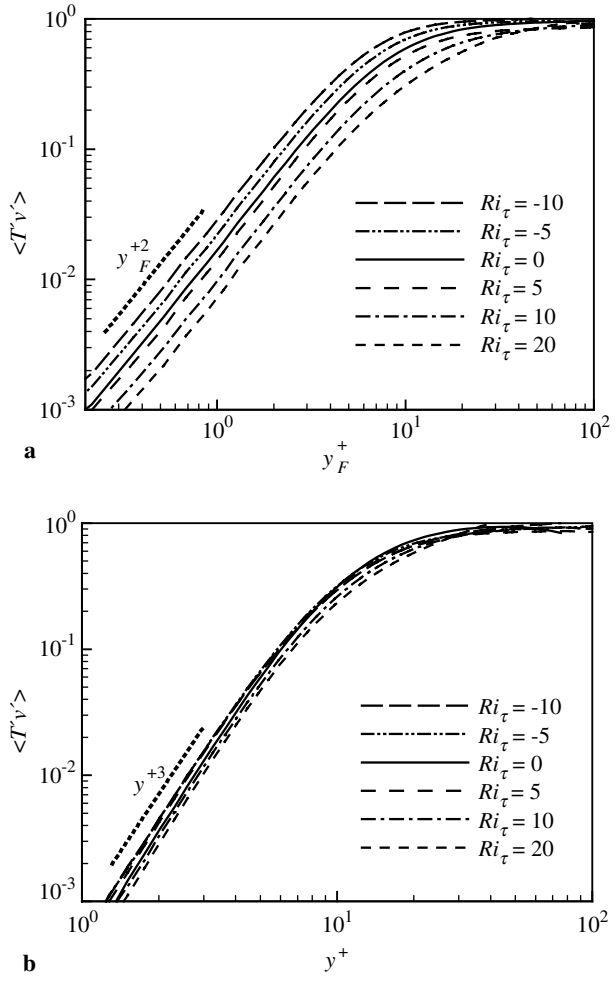

Fig. 9. Profiles of the mean vertical turbulent heat fluxes in the **a** near region of the free surface, and **b** the bottom wall

behavior near the bottom wall agrees well with the results of the stratified turbulent channel flows [27], [28].

Considering the velocity and temperature boundary conditions, the heat flux $< T'v' >$ can be expanded into power series of y_F^+ near the free surface and of y^+ near the bottom wall,

$$\begin{aligned} < T'v' > &= a_1 y_F^{+^2} + a_2 y_F^{+^3} + ..., \quad \text{near the free surface,} \\ < T'v' > &= b_1 y^{+^3} + b_2 y^{+^4} + ..., \quad \text{near the bottom wall.} \end{aligned} \tag{11}$$

Then, both curves of the square and cubic laws with the vertical distance from the free surface (i.e., y_F^+) or from the bottom wall (i.e., y^+) are plotted in Fig. 9 with logarithmic scales to illustrate the first terms in Eqs. (11). As expected, the turbulent heat flux in the vertical direction agrees well with the leading terms behavior in Eqs. (11) in the near regions of the free surface and the wall, respectively.

4.3 Turbulence budgets

To examine the mechanism by which stable (or unstable) stratification suppresses (or enhances) turbulence, it is necessary to analyze the budget terms in the transport equations of the

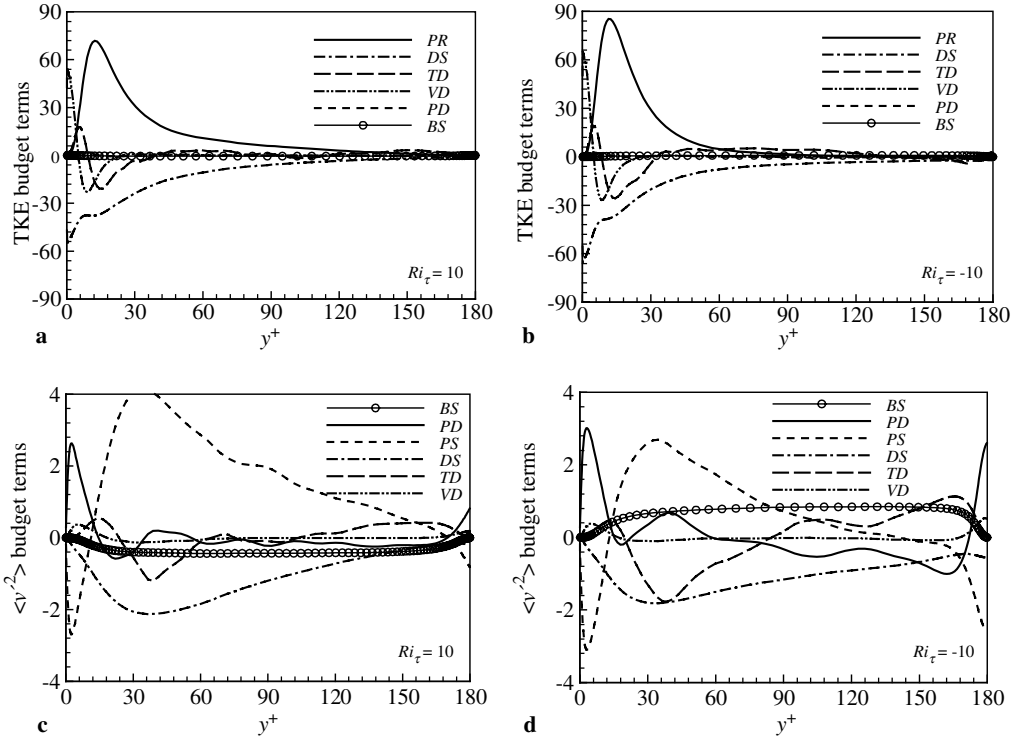

Fig. 10. Budget terms in the transport equations of the turbulent kinetic energy for **a** $\mathrm{Ri}_\tau = 10$ and **b** -10, and of the vertical Reynolds stress for **c** $\mathrm{Ri}_\tau = 10$ and **d** -10

turbulent kinetic energy, or TKE, (i.e., $< u_i' u_i' >$) and the Reynolds stresses (i.e., $< u_i' u_j' >$), which are listed in the Appendix. Due to the inhomogeneity introduced by the wall and the free surface, the terms in the budgets have a strong dependence on the distance from the wall, and the primary balance involves different terms at different heights. The TKE budget terms, referred to in Eq. (A.1), are shown in Fig. 10a and b for $\mathrm{Ri}_\tau = 10$ and -10, respectively. In the near wall region ($y^+ < 40$), the budget balance mainly holds for the terms of *PR*, *DS*, *TD* and *VD*, and both the terms of *PD* and *BS* are small for stable and unstable stratification. The production *PR* for $\mathrm{Ri}_\tau = -10$ is larger than that for $\mathrm{Ri}_\tau = 10$ at $y^+ = 15$ approximately; other terms including *DS*, *TD* and *VD* adjust accordingly.

The turbulence intensities in Fig. 5 exhibit a strong anisotropy near the shear free boundary. To explore the mechanism of the anisotropic behavior, we can examine the distributions of the energy production *PR* and viscous dissipation *DS* in Fig. 10a and b. Although turbulence is produced everywhere in the open channel flow, an analysis of the turbulence kinetic energy balances reveals that the turbulence production in the region $y^+ > 90$ is at least one order of magnitude less than its peak value near the bottom wall. The behavior is certainly in accordance with the experiments [2]–[4] that have shown that surface renewal events have their origin principally in the region of the wall.

Further insights as to how stratification affects the TKE can be obtained by comparing the budgets that contain buoyancy effect terms. The budgets of the vertical Reynolds stress $< u_2'^2 >$ (or $< v'^2 >$), referred to in Eq. (A.2), are shown in Fig. 10c and d for $\mathrm{Ri}_\tau = 10$ and -10, respectively. To view the distributions of the buoyancy effect term *BS*, the *BS* term for $\mathrm{Ri}_\tau = 10$

is negative over the channel and acts as a sink term in the $< v'^2 >$-equation to suppress turbulence. In contrast to the case of $\mathrm{Ri}_\tau = 10$, the BS term for $\mathrm{Ri}_\tau = -10$ is positive and plays as a source term in the $< v'^2 >$-equation to enhance turbulence. In the near wall region ($y^+ < 15$), the budget balance mainly holds for the terms of *PD* and *PS* for stable and unstable stratification. In the region of $y^+ > 15$ approximately, the pressure-strain redistribution term *PS* plays as an important action for the balance of these terms, in particular near the free surface. Meanwhile, the pressure transport *PD* and the turbulent transport rate *TD* for $\mathrm{Ri}_\tau = -10$ become stronger than for $\mathrm{Ri}_\tau = 10$ over the channel.

To clearly exhibit the buoyancy effect near the wall and the free surface, as shown in the above the buoyancy effect term is represented as $2Ri_\tau < T'v' >$, thus, the profiles in Fig. 9, when multiplied by $2\,\mathrm{Ri}_\tau$, represent the absolute value of the budget term induced by the buoyancy force. The difference among these budget terms is more evident near the free surface. It is also indicated that these budget terms reasonably predict the evolution of the vertical turbulent intensity due to the influence of the buoyancy force.

To further analyze the mechanism of strong anisotropy near the free surface, it has been revealed that anisotropic dissipation and pressure-strain effects [13], [20] as well as turbulence structures under the free surface [33] are principally responsible for the anisotropy. Near the free surface, the dissipation becomes anisotropic due to the nature of the shear-free surface boundary conditions. Thus, the vertical fluctuation is preferentially dissipated, leading to an increase in stress anisotropy. To elucidate the effect of the pressure-strain on the energy transfer and anisotropy character near the free surface, the pressure-strain tensor is described as

$$\phi_{ij} = \left\langle p' \left(\frac{\partial u_i'}{\partial x_j} + \frac{\partial u_j'}{\partial x_i} \right) \right\rangle. \tag{12}$$

The trace of this tensor (ϕ_{ij}) is always zero because of the incompressibility constraint. The distributions of the pressure-strain terms versus the vertical distance from the free surface are shown in Fig. 11 for $\mathrm{Ri}_\tau = 10$, 0 and -10. Generally, the value of the pressure-strain in the streamwise direction (ϕ_{11}) near the free surface is smaller than the value of the pressure-strain in the spanwise direction (ϕ_{33}) and is near zero on the free surface, while ϕ_{33} increases in the vicinity of the free surface and remains positive. The pressure-strain in the vertical direction (ϕ_{22}) decreases near the free surface and its sign changes from positive to negative. The sign changing location from positive to negative (i.e., $\phi_{22} = 0$) moves away from the free surface when Ri_τ changes from 10 to -10. The absolute values of ϕ_{22} and ϕ_{33} at the free surface decrease with increasing Ri_τ from -10 to 10. These pressure-strain distributions also indicate that the inter-component energy transfer between the vertical and spanwise direction is deactivated for stable stratification and activated for unstable stratification. It is noted that the turbulence energy in the vertical direction is mainly transferred into the spanwise direction through the pressure-strain effect, in particular for unstable stratification. Thus, as shown in Fig. 5, the turbulence intensity in the spanwise direction increases obviously near the free surface.

4.4 Turbulence structures near the free surface

Turbulent statistics near the free surface stems from the complex turbulent structures, and a large fraction of surface-renewal events originate from the buffer region of the wall boundary layer [5]–[7]. To understand the processes involved in the transport of heat at the free surface, it is necessary to investigate the relationship between the surface thermal field and the velocity and temperature fluctuations. As is well known, the turbulence energy production in the turbulent boundary layer is mainly generated due to the quasi-streamwise vortices, which are the

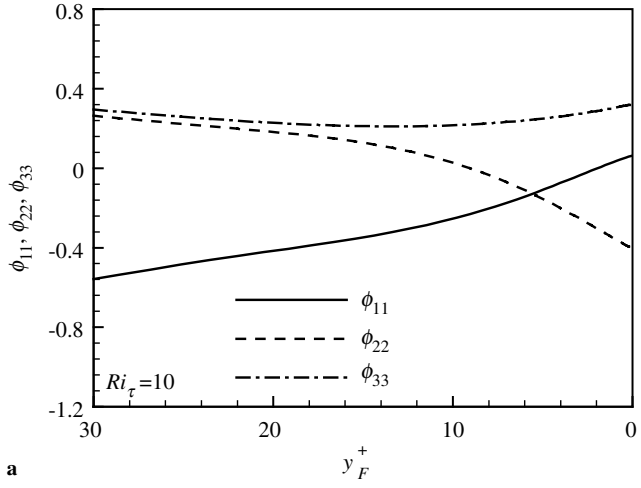

a

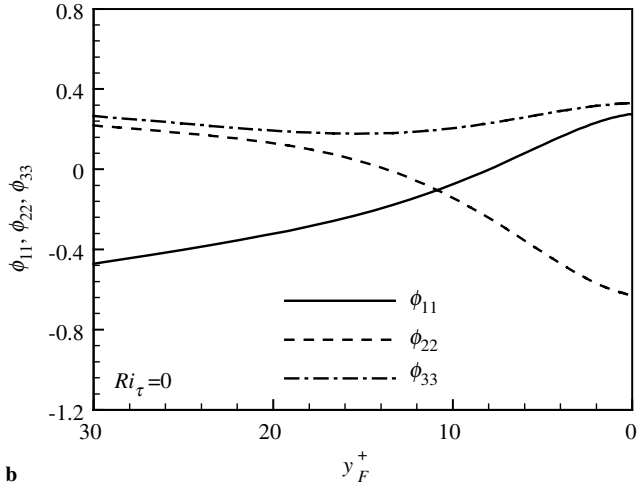

b

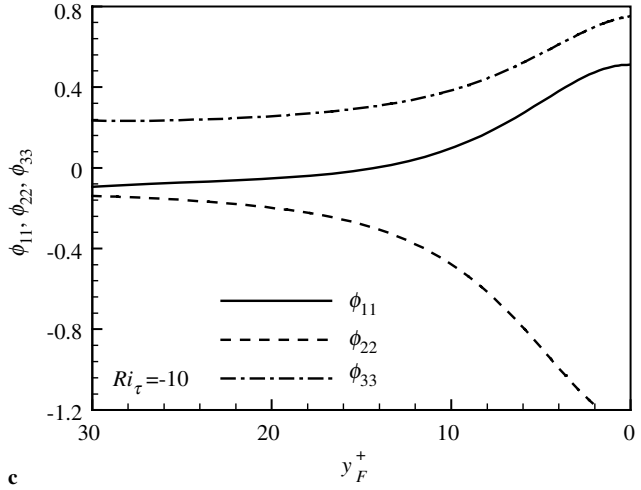

c

Fig. 11. Distributions of the pressure-strain terms for **a** $\mathrm{Ri}_\tau = 10$, **b** 0, and **c** -10

typical coherent structures in the wall turbulence. As shown in Fig. 5, the profiles of the velocity fluctuations near the bottom wall clearly exhibit the influence of stable and unstable stratification on turbulence intensities. According to the contours of the instantaneous streamwise velocity fluctuation near the bottom (not shown here), it is found that, compared to unstratified flow, the formation of streaks is clearly suppressed for stably stratified flow and enhanced for unstably stratified flow. The important processes of bursting, ejection and sweep, consisting of strong vertical motions, are remarkably affected by the stratification effect; therefore, the presence of stable (or unstable) stratification suppresses (or enhances) the generation of bursting motions in the turbulent wall boundary layer. Further, the stratification effect has a significant influence on the surface-renewal motions, because the most bursting eddies generated in the turbulent boundary layer near the bottom wall evolve into the surface-renewal motions.

Figure 12 shows patterns of the instantaneous streamwise and vertical velocity fluctuation near the free surface at $y_F^+ = 0.5$ for $\mathrm{Ri}_\tau = 10$, 0 and -10. Compared to Fig. 12c and d for $\mathrm{Ri}_\tau = 0$, when stable stratification is imposed, as shown in Fig. 12a and b for $\mathrm{Ri}_\tau = 10$, it can be seen that the absent streaky structure near the free surface is formed. Correspondingly, when unstable stratification is activated, the dense streaky structure near the free surface is visualized in Fig. 12e and f for $\mathrm{Ri}_\tau = -10$. As is well known, the structure-renewal motions are mainly generated in the turbulent boundary layer over the bottom wall for unstratified turbulent flow (Komori et al. [2]). Actually, as shown in Fig. 12, this strong interaction between the organized structure in the turbulent boundary layer and the surface-renewal motions near the free surface is also observed in the stratified turbulent flows. Meanwhile, as described in the above, the turbulent boundary layer is relaminarized by the stable stratification, and the intercomponent energy transfer is deactivated. The depression of the surface-renewal motions near the free surface is a direct result of the relaminarization of the turbulent boundary layer in Fig. 12a and b. However, the turbulence near the wall is strengthened due to unstable stratification. Thus, as shown in Fig. 12e and f, the surface-renewal motions near the free surface are enhanced as the intercomponent energy transfer is activated.

The corresponding instantaneous temperature fluctuation and vertical turbulent heat flux fields in the same plane in Fig. 12 are shown in Fig. 13 for $\mathrm{Ri}_\tau = 10$, 0 and -10. One can identify the local spots in accordance with the high- and low-temperature regions alternately. These observations imply that the turbulent mixing of temperature is controlled by the turbulence dynamics near the free surface. By comparing with the flow structures in Fig. 12, it can be observed by noting the almost exact correspondence between the vertical velocity fluctuation in Fig. 12 and the vertical turbulent heat flux in Fig. 13. Based on the flow structures near the free surface, the local spots result in the complicated interaction between the streamwise vortices. As the vortices are mainly aligned in the streamwise direction, the structures hardly transfer turbulence energy to the streamwise direction, which is also confirmed based on the turbulent budget analysis shown above. The organized structure near the free surface usually corresponds to the surface renewal motion [3], patchy structure [7], and hairpin-like eddies [13]. In addition, when heat transfer is considered here, as a typical case for $\mathrm{Ri}_\tau = -10$, the heat can be transported from the wall toward the free surface due to the upward flow. Thus, the upward fluid elements carry with them the higher temperatures associated with the subsurface flow, and must therefore be significantly warmer than the average surface temperature to form the so-called "hot spots", as shown in Fig. 13e. Meanwhile, the corresponding structures in the vertical turbulent heat flux are formed in Fig. 13f.

The eruption process of fluid from the bottom wall region usually retains their coherence in the sequence of convecting toward the free surface. To exhibit the stratification effect on the

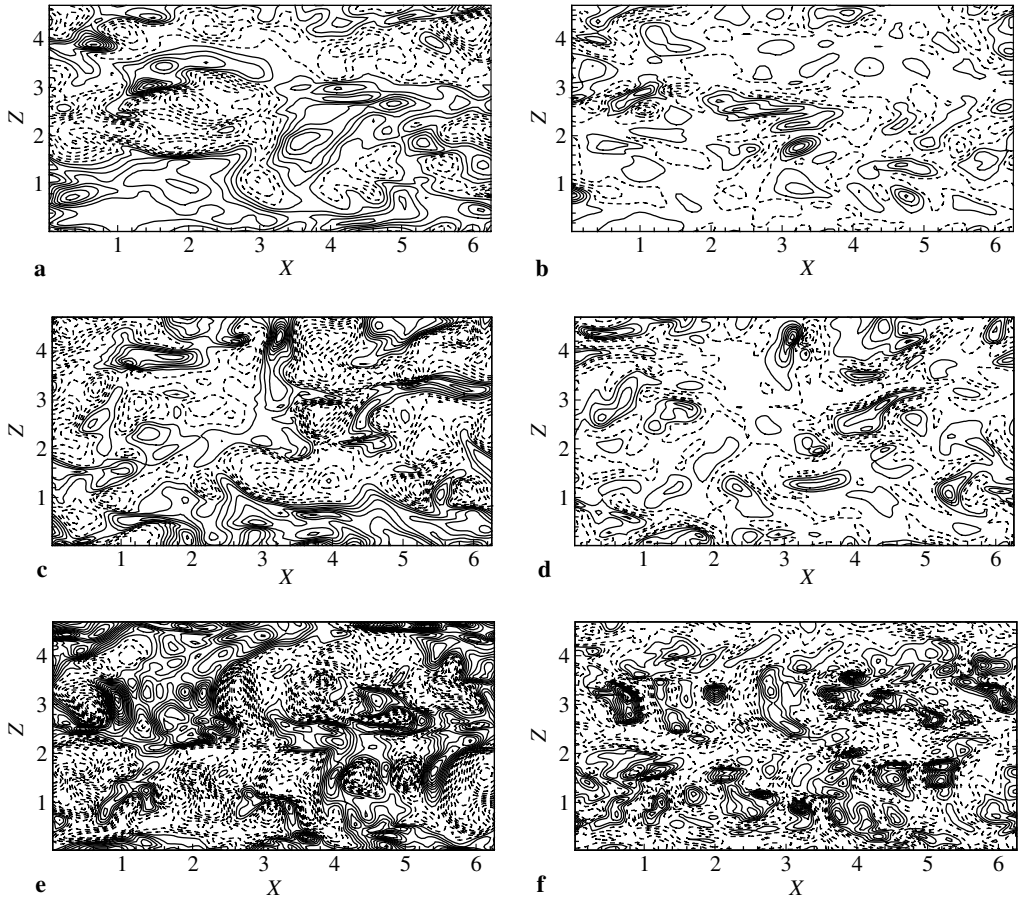

Fig. 12. Contours of the instantaneous streamwise (u') and vertical (v') velocity fluctuation near the free surface at $y_F^+ = 0.5$ for $\mathrm{Ri}_\tau = 10$, 0 and -10: **a** u' and **b** v' for $\mathrm{Ri}_\tau = 10$, **c** u' and **d** v' for $\mathrm{Ri}_\tau = 0$, **e** u' and **f** v' for $\mathrm{Ri}_\tau = -10$

vertical motions, Fig. 14 shows the flow patterns of the instantaneous vertical velocity fluctuation v' and the velocity vector based on v' and w' in a cross plane (i.e., $y - z$ plane) for $\mathrm{Ri}_\tau = 10$, 0 and -10. The absent and dense streaky structures demonstrate the strength of the vertical velocity fluctuation and are consistent with the profiles of the turbulence intensity in Fig. 5b. Compared to unstratified flow in Fig. 14c for $\mathrm{Ri}_\tau = 0$, the dissociation of the streaklike structures near the free surface, as shown in Fig. 14a for $\mathrm{Ri}_\tau = 10$, means that the frequency of the bursting eddies decreases in the stably stratified turbulent flows [35]. However, as shown in Fig. 14e for $\mathrm{Ri}_\tau = -10$, the surface-renewal motions near the free surface are enhanced due to the unstable stratification effect. The organized streaks of the vertical velocity fluctuation exhibit the coherent structures due to the succession of ejection and sweeping events.

From the velocity vector near the free surface in Fig. 14b, d and f in a cross plane for $\mathrm{Ri}_\tau = 10$, 0 and -10, respectively, the regions of the splatting events, where positively large vertical velocity fluctuation is observed near the free surface, are clearly exhibited and enhanced for unstable stratification. This structure contributes to the intercomponent energy transfer from the vertical to the free surface parallel direction by the pressure-strain effects in consis-

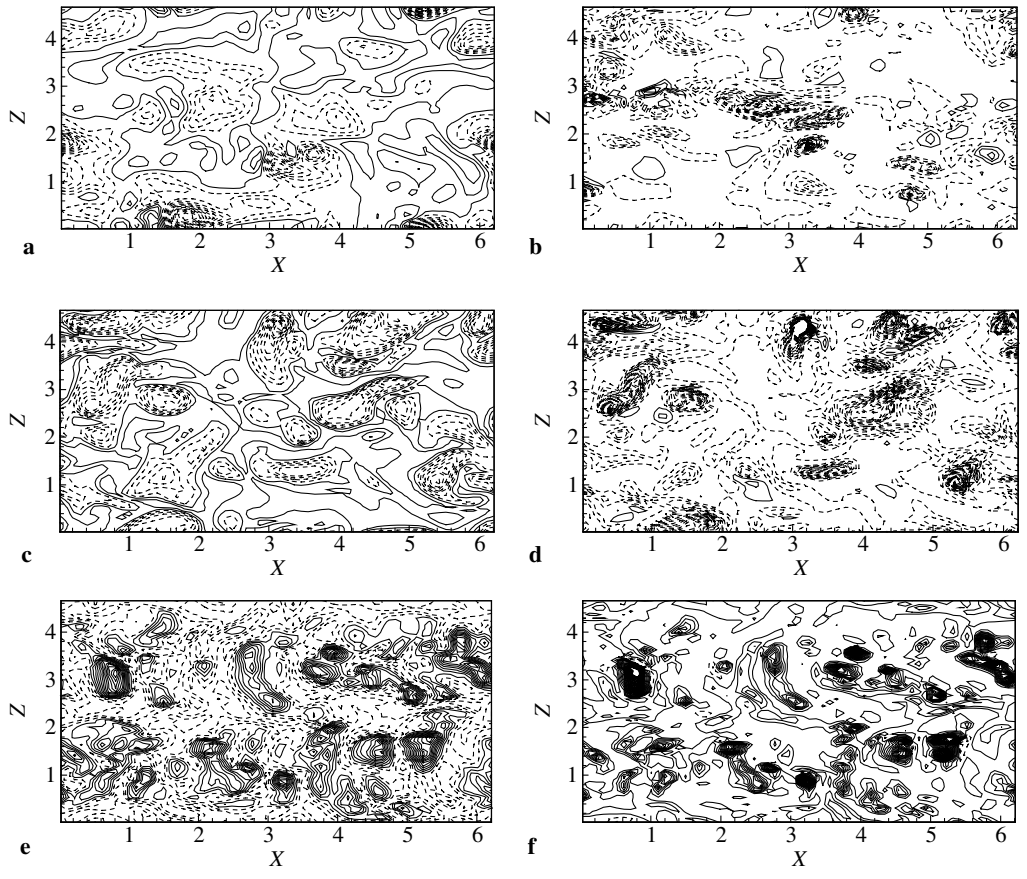

Fig. 13. Contours of the instantaneous temperature fluctuation (T') and vertical turbulent heat flux ($T'v'$) velocity near the free surface at $y_F^+ = 0.5$ for $\mathrm{Ri}_\tau = 10$, 0 and -10: **a** T' and **b** $T'v'$ for $\mathrm{Ri}_\tau = 10$, **c** T' and **d** $T'v'$ for $\mathrm{Ri}_\tau = 0$, **e** T' and **f** $T'v'$ for $\mathrm{Ri}_\tau = -10$

tency with the results shown in Fig. 11. Meanwhile, continuity requires antisplatting or descending motions from the surface. Thus, antisplatting events, where negatively large vertical velocity fluctuation is displayed, are usually encountered on the free surface. However, the turbulence energy is mainly transferred from the vertical to the spanwise direction near the free surface, as indicated in Fig. 11. Thus, the splatting events should play a dominating role for the intercomponent energy transfer between the vertical and the surface-parallel directions near the free surface, in particular for unstable stratification.

5 Conclusions

Direct numerical simulation of stably and unstably stratified turbulent open channel flow has been performed. The three-dimensional Navier-Stokes and energy equations under the Boussinesq approximation are numerically solved using a fractional-step method coupled with the high-order accurate spatial schemes. The decisive validation of the present approach has been achieved by comparing our calculated results with some available computational and experimental results.

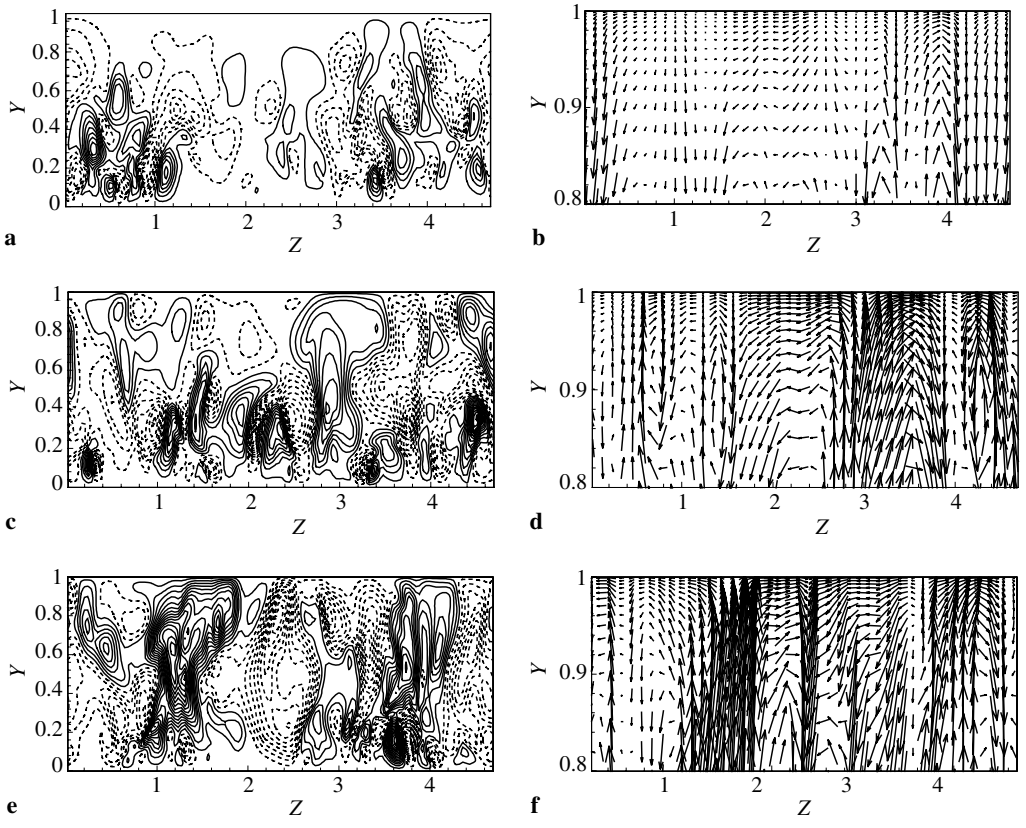

Fig. 14. Contours of the instantaneous vertical velocity fluctuation v' and the velocity vector based on v' and w' in a cross plane: **a** v' contours and **b** $v' - w'$ vectors for $\mathrm{Ri}_\tau = 10$, **c** v' contours and **d** $v' - w'$ vectors for $\mathrm{Ri}_\tau = 0$, **e** v' contours and **f** $v' - w'$ vectors for $\mathrm{Ri}_\tau = -10$

Based on our calculated results, effects of thermally stable and unstable stratification on the characteristics of turbulent flow and heat transfer and on turbulence structures near the free surface are investigated. There still exists a buffer layer followed by a logarithmic region in the mean velocity profile near the bottom wall. As the influence of the stratification, it is reasonably predicted that the von Kárman constant and the additive constant in the log law of the velocity profile decrease when the Richardson number increases from -10 (i.e., unstable stratification) to 20 (i.e., stable stratification). Similarly, the mean temperature has the same behavior as the mean velocity for the variation of the von Kárman constant and the additive constant in the log law of the temperature profile versus the Richardson number. Based on the mean temperature profiles near the free surface, it is revealed that the Nusselt number at the free surface decreases when the Richardson number increases and an approximately linear relationship between the Nusselt number and the Richardson number appears.

Turbulence intensities are reduced due to stable stratification and enhanced due to unstable stratification. Following the analysis of the budget terms in the transport equations of the turbulent kinetic energy and the vertical Reynolds stress, the buoyancy effect is to suppress turbulence for stable stratification and to enhance turbulence for unstable stratification. Meanwhile, the surface-renewal motions near the free surface are strengthened due to unstable stratification and restrained due to stable stratification. The turbulence intensities reveal that

turbulent flow has a strong anisotropy near the shear free boundary. The turbulence energy in the vertical direction is transferred into the free surface parallel directions through the pressure-strain effect, in particular for unstable stratification. Meanwhile, the energy transfer is not homogeneous in the two surface parallel directions due to the presence of the streamwise vortices. These vortices also contribute to the surface renewal at the free surface and control heat transfer there.

Appendix

Equations for statistical quantities

The equation for the turbulent kinetic energy (TKE) $q^2 =< u_i' u_i' >$ for the open channel flow can be written as (nondimensionalized as above)

$$\frac{\partial q^2}{\partial t} = PR + DS + TD + VD + PD + BS, \tag{A1}$$

where the terms on the right-hand side are

$PR = -2 < u_1' u_2' > d < u_1 > /dy$ production of TKE;

$DS = -2/\mathrm{Re}_\tau < (\partial u_i'/\partial x_j)(\partial u_i'/\partial x_j) >$ viscous dissipation;

$TD = -d[< (u_i')^2 u_2' >]/dy$ turbulent transport;

$VD = 1/\mathrm{Re}_\tau d^2(< u_i' u_i' >)/dy^2$ viscous diffusion;

$PD = -2d(< p' u_2' >)/dy$ pressure transport;

$BS = 2\mathrm{Ri}_\tau < T' u_2' >$ buoyancy effect.

The transport equation for the vertical Reynolds stress ${u'_2}^2$ (or ${v'}^2$) can be obtained as

$$\frac{\partial}{\partial t} < {u'_2}^2 >= PD + PS + DS + TD + VD + BS, \tag{A.2}$$

where the various terms are

$PD = -2d(< p' u_2' >)/dy$ pressure transport;

$PS =< p'(\partial u_2'/\partial y) >$ pressure-strain redistribution;

$DS = -2/\mathrm{Re}_\tau < (\partial u_2'/\partial x_j)(\partial u_2'/\partial x_j) >$ viscous dissipation;

$TD = -d[< (u_2')^3 >]/dy$ turbulent transport rate;

$VD = 1/\ \mathrm{Re}_\tau d^2(< u_2' u_2' >)/dy^2$ viscous diffusion;

$BS = 2\ \mathrm{Ri}_\tau\ < T' u_2' >$ buoyancy effect.

Acknowledgements

This work was supported by the National Natural Science Foundation of China (Nos. 90405007 and 10125210), the China NKBRSF Project (No 2001CB409600), the Specialized Research Fund for the Doctoral Program of Higher Education (No. 20020358013), and the Hundred-Talent Programme of the Chinese Academy of Sciences.

References

[1] Nakagawa, H., Nezu, I.: Structure of space-time correlations of bursting phenomena in open-channel flow. J. Fluid Mech. **104**, 1–43 (1981).

[2] Komori, S., Murakami, Y., Ueda, H.: The relationship between surface-renewal and bursting motions in an open-channel. J. Fluid Mech. **203**, 103–123 (1989).

[3] Komori, S., Nagaosa, R., Muramami, Y.: Turbulence structure and mass transfer across a sheared air-water interface in wind driven turbulence. J. Fluid Mech. **249**, 161–183 (1993).

[4] Kumar, S., Gupta, R., Banerjee, S.: An experimental investigation of the characteristics of free-surface turbulence in channel flow. Phys. Fluids **10**, 437–456 (1998).

[5] Rashidi, M., Banerjee, S.: Turbulence structure in free surface flows. Phys. Fluids **31**, 2491–2503 (1988).

[6] Rashidi, M., Hetstroni, G., Banerjee, S.: Mechanisms of heat and mass transport at gas-liquid interfaces. Int. J. Heat Mass Transf. **34**, 1799–1805 (1991).

[7] Rashidi, M.: Burst-interface interactions in free surface turbulent flows. Phys. Fluids **9**, 3485–3501 (1997).

[8] Lam, K., Banerjee, S.: On the condition of streak formation in a bounded turbulent flow. Phys. Fluids **4**, 306–320 (1992).

[9] Komori, S., Nagaosa, R., Murakami, Y., Chiba, S., Ishii, K., Kuwahara, K.: Direct numerical simulation of three-dimensional open-channel flow with zero-shear gas-liquid interface. Phys. Fluids **5**, 115–125 (1993).

[10] Pan, Y., Banerjee, S.: A numerical study of free-surface turbulence in channel flow. Phys. Fluids **7**, 1649–1664 (1995).

[11] Lombardi, P., De Angelis, V., Banerjee, S.: Direct numerical simulation of near-interface turbulence in coupled gas-liquid flow. Phys. Fluids **8**, 1643–1665 (1996).

[12] Nagaosa, R.: Direct numerical simulation of vortex structures and turbulent scalar transfer across a free surface in a fully developed turbulence. Phys. Fluids **11**, 1581–1595 (1999).

[13] Handler, R. A., Saylor, J. R., Leighton, R. I., Rovelstad, A. L.: Transport of a passive scalar at a shear-free boundary in fully developed turbulent open channel flow. Phys. Fluids **11**, 2607–2625 (1999).

[14] Handler, R. A., Leighton, R. I., Smith, G. B., Nagaosa, R.: Surfactant effects on passive scalar transport in a fully developed turbulent flow. Int. J. Heat Mass Transf. **46**, 2219–2238 (2003).

[15] Shen, L., Zhang, X., Yue, D. K. P., Triantafyllou, G. S.: The surface layer for free-surface turbulent flows. J. Fluid Mech. **386**, 167–212 (1999).

[16] Shen, L., Triantafyllou, G. S., Yue, D. K. P.: Mixing of a passive scalar near a free surface. Phys. Fluids **13**, 913–926 (2001).

[17] Komori, S., Ueda, H., Ogino, F., Mizushina, T.: Turbulence structure in stably stratified open-channel flow. J. Fluid Mech. **130**, 13–26 (1983).

[18] Gerz, T., Schumann, U., Elgobashi, S. E.: Direct numerical simulation of stratified homogeneous turbulent shear flows. J. Fluid Mech. **200**, 563–594 (1989).

[19] Holt, S. E., Koseff, J. R., Ferziger, J. H.: A numerical study of the evolution and structure of homogeneous stably stratified sheared turbulence. J. Fluid Mech. **237**, 499–539 (1992).

[20] Nagaosa, R., Saito, T.: Turbulence structure and scalar transfer in stratified free-surface flows. AIChE J. **43**, 2393–2404 (1997).

[21] Verzicco, R., Orlandi, P.: A finite-difference scheme for three-dimensional incompressible flows in cylindrical coordinates. J. Comput. Phys. **123**, 402–414 (1996).

[22] Rai, M. M., Moin, P.: Direct simulation of turbulent flow using finite-difference schemes. J. Comput. Phys. **96**, 15–53 (1991).

[23] Dong, Y. H., Lu, X. Y., Zhuang, L. X.: Large eddy simulation of turbulent channel flow with mass transfer at high-Schmidt numbers. Int. J. Heat Mass Transf. **46**, 1529–1539 (2003).

[24] Dong, Y. H., Lu, X. Y.: Large eddy simulation of a thermally stratified turbulent channel flow with temperature oscillation on the wall. Int. J. Heat Mass Transf. **47**, 2109–2122 (2004).

[25] Wang, L., Lu X. Y.: An investigation of turbulent oscillatory heat transfer in channel flows by large eddy simulation. Int. J. Heat Mass Transf. **47**, 2161–2172 (2004).

[26] Liu, N. S., Lu, X. Y.: Large eddy simulation of turbulent concentric annular channel flows. Int. J. Numer. Meth. Fluids **45**, 1317–1338 (2004).

[27] Garg, R. P., Ferziger, J. H., Monismith, S. G., Koseff, J. R.: Stably stratified turbulent channel flows. I. Stratification regimes and turbulence suppression mechanism. Phys. Fluids **12**, 2569–2594 (2001).
[28] Armenio, V., Sarkar, S.: An investigation of stably-stratified turbulent channel flow using large eddy simulation. J. Fluid Mech. **459**, 1–42 (2002).
[29] Arya, S. P. S.: Buoyancy effects in a horizontal flat-plate boundary layer. J. Fluid Mech. **68**, 321–343 (1975).
[30] Kays, W. M., Crawford M. E.: Convective heat and mass transfer. New York: McGraw-Hill 1987.
[31] Kader, B. A., Yaglom, A. M.: Heat and mass transfer laws for fully turbulent wall flows. Int. J. Heat Mass Transf. **15**, 2329–2342 (1972).
[32] Kader, B. A.: Temperature and concentration profiles in fully turbulent boundary layers. Int. J. Heat Mass Transf. **24**, 1541–1545 (1981).
[33] Perot, B., Moin, P.: Shear-free boundary layers: 1. Physical insights into near wall turbulence. J. Fluid Mech. **295**, 199–227 (1995).
[34] Wang, L., Dong, Y. H., Lu, X. Y.: An investigation of turbulent open channel flow with heat transfer by large eddy simulation. Comp. Fluids **34**, 23–47 (2005).
[35] Hinze, J. O.: Turbulence. New York: McGraw-Hill 1975.

Authors' addresses: Y.-H. Dong, Department of Modern Mechanics, University of Science and Technology of China, Hefei, Anhui 230026, and Shanghai Institute of Applied Mathematics and Mechanics, Shanghai University, Shanghai 200072, China; X.-Y. Lu (corresponding author), Department of Modern Mechanics, University of Science and Technology of China, Hefei, Anhui 230026, China (E-mail: xlu@ustc.edu.cn)